Cyclotron resonance of carbon-doped two-dimensional hole systems: From the magnetic quantum limit to low magnetic fields

K. Rachor,* T. E. Raab, and D. Heitmann
Institut für Angewandte Physik und Zentrum für Mikrostrukturforschung, Universität Hamburg, Jungiusstraße 11, 20355 Hamburg, Germany

C. Gerl and W. Wegscheider
Institut für Angewandte und Experimentelle Physik II, Universität Regensburg, Universitätsstraße 31, 93040 Regensburg, Germany
(Received 15 January 2009; revised manuscript received 11 February 2009; published 18 March 2009)

We report on cyclotron resonance (CR) experiments of high-quality C-doped two-dimensional hole systems in GaAs/AlGaAs quantum wells covering the microwave and far-infrared regimes. At high magnetic field B we observe a strong B dependence of the cyclotron mass m_c which can be reproduced by calculations based on a 4×4 Luttinger Hamiltonian in the axial approximation. At small B one main and up to three secondary CRs are found, which continuously evolve with smooth magnetic-field dependences. This has not been observed and predicted so far. In the regime of the magnetic quantum limit a further CR is observed, which can be attributed to a transition between Landau levels originating from the two different spin-split heavy- and light-hole subbands.

DOI: 10.1103/PhysRevB.79.125417 PACS number(s): 78.67.De, 73.21.Fg

I. INTRODUCTION

The topmost four valence bands in bulk GaAs have an angular momentum $j=3/2$ yielding the twofold degenerated heavy-hole (HH) band with z component of angular momentum $m=\pm3/2$ and the twofold degenerated light-hole (LH) band with $m=\pm1/2$. In quantum wells, size quantization gives rise to the formation of subbands and lifts, therefore, the fourfold degeneracy of HH and LH at the in-plane wave vector $k_{\|}=0$. These subbands are not pure with respect to the z component of angular momentum yielding a strong nonparabolicity of the subband structure for finite $k_{\|}$.[1–3] The resulting effective mass m^* therefore shows a strong dependence on $k_{\|}$, in doped systems, on the Fermi wave vector k_F, and consequently on the hole density p_s. Additional inversion-asymmetry-induced spin splitting turns out to be much more important for two-dimensional hole systems (2DHSs) than for two-dimensional electron systems (2DESs) with respect to their kinetic energies.[4] This is interesting for fundamental reason and also for application, for example, for spintronic devices.

Cyclotron resonance (CR) experiments have been proven to be a powerful tool for revealing different aspects of the complexity of 2DHS.[5–14] At first, 2DHSs in Si-metal-oxide-semiconductor (MOS) structures were investigated.[5] The first CR experiments on GaAs-based 2DHS were performed on Be-doped (100) samples.[6] This publication nicely demonstrated the inversion-asymmetry-induced spin splitting by the detection of two more or less constant cyclotron masses m_c. Further publications about Be-doped 2DHS with high densities also indicated the spin splitting and additionally the nonparabolicity of 2DHS by a dependence of m_c on magnetic field B below the magnetic quantum limit.[7] Using Si as an acceptor for samples grown on (311)-orientated GaAs substrate the fabrication of high-quality 2DHS had become possible. At such samples, the nonparabolicity of 2DHS could be shown at ultralow-density samples.[8] In several publications anticrossings between the Landau levels due to the low symmetry of the (311) direction were observed,[8–12] which, however, makes a comparison with theory very difficult. Other publications dealt with the influence of carrier-carrier interactions on the spin-split CRs.[13] Here, a two-level system was assumed at sufficient low B; thus, that the nonparabolicity did not play an essential role.

For an extensive understanding of 2DHS it is highly desirable to perform CR experiments in a wide range of frequencies and B from the magnetic quantum limit to magnetic fields, where several Landau levels are occupied. The samples must have high quality for sharp resonances. To minimize effects due to anticrossings of the Landau levels samples with high-symmetric growth directions are needed. Recently, it has become possible to fabricate high-mobility 2DHS in the growth direction of high symmetry (001) using carbon as an acceptor.[15–17] The dependence of m_c on the density[18–20] or the quantum-well width[19,20] of such samples has been demonstrated in principle. In the investigated energy regime no dependence of m_c on B was observed.

In this paper we present the results of CR experiments of carbon-doped 2DHS with a gate tunable hole density p_s grown in the (001) direction. We have performed transmission spectroscopy covering the regime of far-infrared (FIR) and microwave (MW) radiation over a wide range of B, so that the evolution of the CR could be observed from the magnetic quantum limit to small magnetic fields. The results are compared with self-consistent calculations based on a 4×4 Luttinger Hamiltonian in the axial approximation.[21] We can clearly and continuously show that for all hole densities there is a strong increase in m_c with B in the high-field regime which can be reasonably described by the theory. The theoretically calculated strong dependence of m_c on B and the positions of the integer filling factors ν for lower fields is not observed. Surprisingly, we rather obtain a continuous evolution of one main and up to three secondary sharp resonances. They do not show any cusps or jumps near integer

filling factors, as observed in electron systems,[22,23] but a smooth dispersion in dependence on B.

In addition, we observe a weak but clearly resolved resonance, which will be attributed to a transition between Landau levels originating from the two different spin-split heavy- and light-hole subbands. This resonance appears in the regime of the magnetic quantum limit and disappears with decreasing B and has a relatively low cyclotron mass of about $0.15m_e$.

The paper is organized as follows. In Sec. II we describe the sample and our experimental setup. The CR measurements and results are presented in Sec. III followed by a brief description of the theory in Sec. IV. We discuss our results in Secs. V A and V B by comparing them with the theory for high and low magnetic fields. In addition, the CR between Landau levels of different subbands is discussed in Sec. V C. In Sec. V D we demonstrate a similar behavior in the strong temperature dependence of transport and cyclotron mobility. We conclude in Sec. VI.

II. SAMPLE PREPARATION AND EXPERIMENTAL SETUP

In this work we measure the CR of a 2DHS which is confined in a single-sided modulation-doped nominally 15-nm-wide quantum well grown by molecular-beam epitaxy on a (001)-orientated GaAs substrate using carbon as an acceptor. Photoluminescence (PL) measurements revealed a width of the quantum well of 14.5 nm.[24] The upper and lower barriers are determined by $Al_{0.3}Ga_{0.7}As$. The carbon δ-doping layer is separated by an 80 nm spacer in the upper layer. Contacts were prepared by soldering an alloy of indium and zinc (96:4) onto the mesa followed by an annealing process at 350 °C for 1 min. A 3×3 mm^2 titanium gate, which is transparent for the FIR and MW radiation, was evaporated allowing a tuning of the hole density p_s between 0.7×10^{11} and 1.6×10^{11} cm^{-2}. This range was limited by the onset of strong leakage currents. p_s was determined by both the absorption strengths of the CR and the magnetocapacitance measurements. The zero-field transport mobility at a temperature of $T=1.6$ K measured at another sample of the same wafer was $\mu_{tr}=1.1\times10^6$ cm^2/V s demonstrating the high quality of the sample. The substrate was wedged at an angle of 2° to suppress Fabry-Perot interferences in the FIR spectrum.

Due to the large cyclotron mass of the holes (up to $0.41m_e$ in our experiments with perpendicular magnetic field $B=0-14$ T) and its strong variations we have to cover a large frequency range spanning the low FIR and the MW regimes, which is quite an experimental challenge. In our experiments we use both a Fourier-transform spectrometer (FTS) and a tunable microwave generator with several frequency multipliers. The sample is mounted in the center of a 14 T superconducting magnet. We use the Faraday configuration, i.e., the FIR radiation is irradiated perpendicular to the sample and parallel to the magnetic field. A variable temperature insert (VTI) allows us to tune the temperature of the sample. In our measurements we range the temperature between 1.6 and 12 K.

The Bruker 113v FTS with a broadband Hg lamp covers the frequency range above about 1.30 meV (315 GHz) using 125 and 50 μm beam splitters in its Michelson interferometer. The FIR light is guided through a 10 mm light pipe to the sample and the transmitted light is detected by a Si bolometer cooled to 2.2 K. With the FTS we measure simultaneously the frequencies at fixed magnetic fields.

For the experiments at lower frequencies we use a tunable MW generator with a frequency range from 100 kHz to 70 GHz and four different frequency multipliers which allows us to cover, except for a small gap between 0.7 and 0.9 meV (170–220 GHz), the whole frequency range up to 1.34 meV, i.e., we have overlap with the sensitivity regime of the FTS. The diameter of the light pipe limits the lowest transmitted energy to 0.33 meV. In the MW experiments we fix the frequencies and sweep the magnetic field. We use the same light pipe setup and bolometer as for the FIR experiments, which allows us to perform the measurements without dismantling and warming up the sample.

Note that it is a real challenge to cover such a broad frequency range in one setup. It is nearly impossible to avoid interference and cavity effects over this regime due to impedance mismatches. However, we found that a small modulation of the MW frequency ($\Delta f=9$ GHz) improved the quality of the spectra significantly (in particular the resonance profile).[25] Also it is not possible to control the polarization and we have neither for the MW nor the FIR experiment a perfectly unpolarized radiation. In the MW range we have rather a frequency-dependant degree of circular polarization. Note that experiments with well-defined circular polarization over such broad frequency ranges are quite rare in the field of spectroscopy on low-dimensional systems.[26]

III. CYCLOTRON RESONANCE MEASUREMENTS

Figure 1(a) shows a summary of measured transmission spectra in the FIR regime at a temperature of $T=1.6$ K for different fixed magnetic fields B. We evaluate the normalized transmission $T_N(\omega)=T(\omega,B)/T(\omega,B_0)$, where B_0 is a magnetic field outside the regime of the cyclotron resonance. We observe that the position of the cyclotron resonance at high magnetic fields shifts much stronger with increasing B than that at small fields, which arises from the strong nonparabolicity of the hole band structure yielding a clearly varying cyclotron mass. We will discuss this point in detail later. The higher magnetic fields represent the region of the magnetic quantum limes (filling factor $\nu<1$). There a very narrow cyclotron resonance is observed with a full width at half maximum (FWHM) of about 0.037 meV (0.3 cm^{-1}) or, translated into a cyclotron mobility, $\mu_{CR}=2\times10^5$ cm^2/V s. The low magnetic fields represent the regime of $1<\nu<2$. There the cyclotron resonance is broadened by a factor of 2–3 compared to the case of the magnetic quantum limit. Note that both the necessity of measuring with high resolution and the low intensity at the low-energy operational limit of the Fourier spectrometer reduce the signal-to-noise ratio.

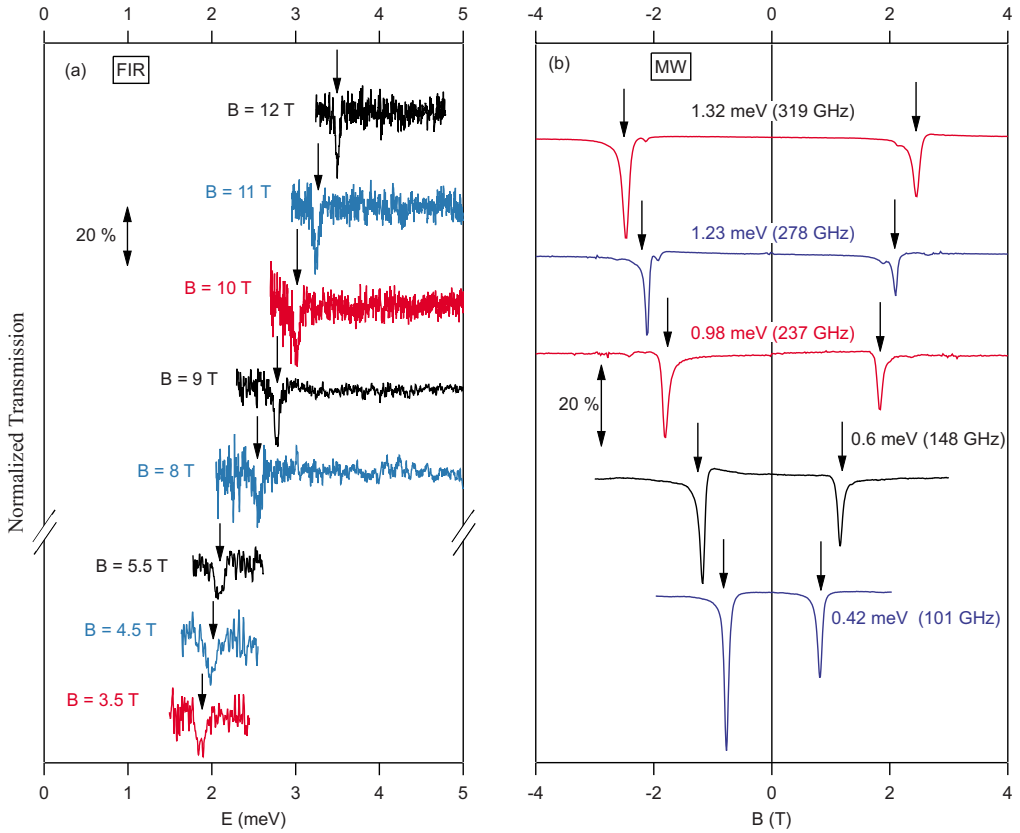

FIG. 1. (Color online) Experimental spectra in the (a) FIR and (b) MW regimes at 1.6 K for a 15-nm-wide quantum well at $p_s = 1.3 \times 10^{11}$ cm^{-2}. (a) Experimental spectra for different fixed fields B. The spectra are normalized to other magnetic fields with resonances far away from the resonance under investigation and are offset for clarity. Arrows indicate the CR. Between $B = 5.5$ and 8 T the CR is not on display: due to the reduced beam-splitter efficiency the signal-to-noise ratio is quite low in the regime of 2.1–2.5 meV. The positions of the cyclotron resonance shifts stronger for higher magnetic fields than for lower fields. The resonance clearly broadens at lower magnetic fields. (b) Experimental spectra for different fixed MW frequencies. Note that in contrast to (a) the measurements in the MW regime were performed at fixed frequencies while sweeping the magnetic field. The spectra are normalized to the transmission signal at $B = 0$ T and are offset for clarity. Arrows indicate the cyclotron resonance. The additional resonances which appear next to the indicated resonances are discussed later in the text.

Figure 1(b) shows a compendium of measured spectra in the MW regime at $T = 1.6$ K for a large range of different MW energies. Note that in contrast to the measurements in the FIR regime the energy is fixed while the magnetic field is swept. We want to first focus on the main resonance which is indicated by arrows and which we associate again with the cyclotron resonance. There are additional resonances which appear next to the indicated cyclotron resonances. They are discussed later in the text. The drastically increased signal-to-noise ratio compared to the FIR data results from the much higher intensity of the MWs. In contrast to the results in the FIR regime, in the MW regime the CR does not show an exactly symmetric line shape, which can be seen, for example, in the measurement for $E = 0.61$ meV. As mentioned before, we believe that this arises from the interference and cavity effects in the setup because its dimensions are of the same order as the wavelength of the microwaves. It turned out that to determine the position, width, and depth of the resonance a fitting expression for the transmission $T(B)$ can be used which consists of a symmetric Lorentz function and an antisymmetric contribution,

$$T(B) = 1 - \left(a_{\mathrm{sym}} \frac{(\Delta B/2)^2}{(B - B_0)^2 + (\Delta B/2)^2} + a_{\mathrm{asym}} \frac{(\Delta B/2)(B - B_0)}{(B - B_0)^2 + (\Delta B/2)^2} \right). \quad (1)$$

a_{sym} and a_{asym} are the amplitudes of, respectively, the symmetric and antisymmetric contributions, where, in general, $a_{\mathrm{asym}}/a_{\mathrm{sym}} \ll 0.2$ in our measurements. ΔB is the width of the CR and B_0 denotes the resonance position. The absolute positions of the CR are the same for both polarizations of the magnetic field whereas the amplitudes are different. This is due to a difference in the intensities of the left- and right-handed circular polarized contributions to the MW radiation which cannot be avoided for our broadband setup.

Figure 2 shows the expanding magnetic-field dispersions of the cyclotron resonance energies E and the corresponding cyclotron mass $m_c = eB\hbar/E$. The dispersions were measured at $T = 1.6$ K at three different hole densities p_s which range from 0.7×10^{11} to 1.6×10^{11} cm^{-2}. Crosses indicate CR measurements with FIR and the open circles indicate those

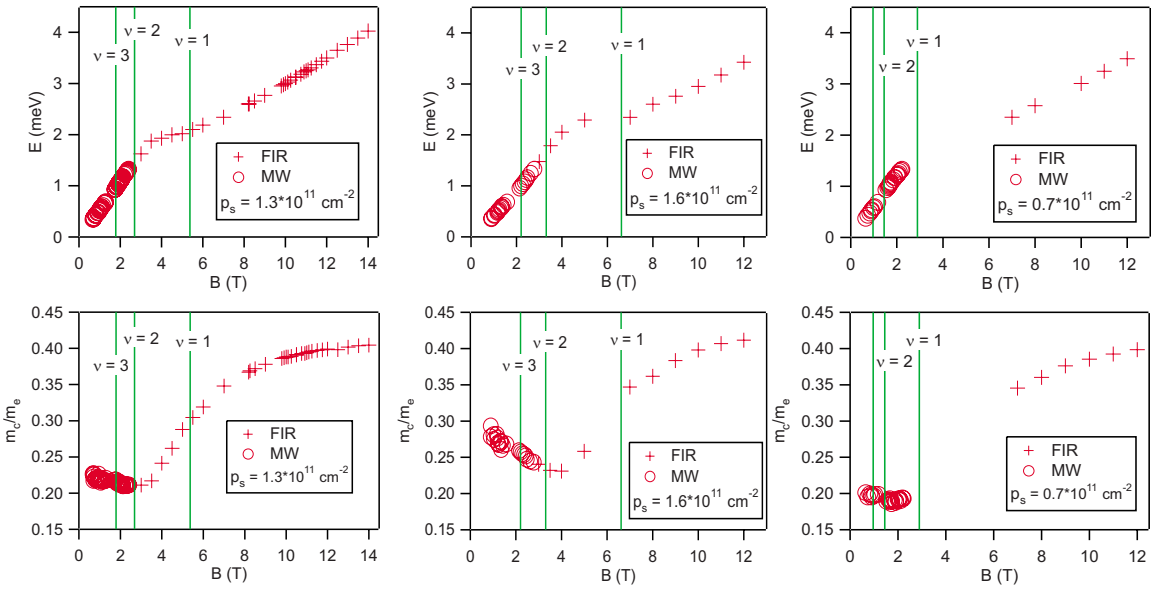

FIG. 2. (Color online) Magnetic-field dependence of the cyclotron resonance energy E and corresponding cyclotron mass m_c measured at $T=1.6$ K for three different hole densities p_s ranging from 0.7×10^{11} to 1.6×10^{11} cm^{-2}. The low-frequency regime will be shown on an expanded scale later. Crosses indicate the CR measured with FIR and the open circles indicate those measured with MW. The small gap in the MW part has experimental reasons. The positions of integer filling factors ν are indicated by perpendicular lines. The dispersion of the cyclotron resonance energy shows for all three hole densities a strongly nonproportional dependence on B which indicates a strong dependence of the cyclotron mass on B. Differences in m_c dispersions for different hole densities are particularly obvious for small magnetic fields B.

with MW. We do not have a frequency multiplier for the regime of 0.7–0.9 meV, so we have no data here. The positions of integer filling factors ν are indicated with perpendicular lines.

E shows a strongly nonlinear magnetic-field dependence at all hole densities resulting in a strong variation of m_c by about a factor 2. This is a substantial difference from dispersions obtained in material systems having a nearly parabolic band structure like two-dimensional electron systems.

We want to first focus on the magnetic-field dependence obtained at $p_s=1.3\times10^{11}$ cm^{-2} shown in the left part of Fig. 2. The dependence of the energy as well as that of the mass can be divided into three regions. At first for $B<4$ T the energy shows a slightly nonlinear dependence on B. The resulting m_c ranges from $0.23m_e$ to $0.21m_e$ with a minimum at about $B=2.2$ T. In the second region between 4 and 6 T E is almost constant. This yields a strong increase in m_c up to $0.35m_e$. In the third region, $B>6$ T, E depends slightly nonlinear on B yielding an asymptotic increase in m_c up to $0.40m_e$. The dispersion for $p_s=1.6\times10^{11}$ and 0.7×10^{11} cm^{-2} can be divided qualitatively into the same three regions. It is worth noting that the almost magnetic-field-independent region of E lies roughly between 4 and 6 T for $p_s=1.3\times10^{11}$ and 1.6×10^{11} cm^{-2}. For the low density of $p_s=0.7\times10^{11}$ cm^{-2} the absorption is correspondingly reduced. Thus we cannot resolve the resonances in the regime of 4 and 6 T. However, from comparison to the measurements at the other hole densities we believe that also for this density a regime exists where E does not depend on B.

A minimum of m_c appears around $\nu=2$ for all hole densities. In the asymptotic regions of high magnetic field m_c depends little on p_s, whereas large differences of m_c are observed in the region of small magnetic fields for different hole densities: at $p_s=1.6\times10^{11}$ cm^{-2} m_c ranges between $0.23m_e$ and $0.29m_e$, whereas at $p_s=0.7\times10^{11}$ cm^{-2} m_c ranges between $0.19m_e$ and $0.20m_e$.

Multiple cyclotron resonances can be expected due to the highly nonparabolic band structure of two-dimensional hole systems[7] and the spin-split band structure[7,6] for $\nu>1$. Indeed our measurement exhibits the main CR described above and multiple secondary CRs at magnetic fields $B<4$ T. We focus on those in the following. These secondary CRs have in general less than 25% of the absorption strength of the main resonance. Typical spectra are shown in Fig. 3 measured at $T=1.6$ K for $p_s=1.3\times10^{11}$ cm^{-2}. Solid arrows indicate the main cyclotron resonances CR, while dashed arrows indicate the secondary CRs. Up to three secondary CRs can be resolved, e.g., for $E=0.48$ meV. The number of secondary CRs varies even over a small frequency range; for example, the spectrum at 1.08 meV exhibits two secondary CRs, whereas the spectrum at 1.03 meV exhibits only the main CR. As for the main CR the absolute magnetic-field positions of the secondary CRs are identical for both directions of the magnetic field, whereas the corresponding amplitudes are different due to the polarization of the MW radiation. In most cases, the secondary CRs are separated from the main CR by more than a factor of 2 of its linewidth.

Figure 4 shows the magnetic-field dependence of the main and secondary cyclotron resonance energies E and the resulting cyclotron mass m_c for $B<4$ T for the same hole densities that are on display in Fig. 2. For all three hole densities p_s the secondary cyclotron resonances' energies E can be clearly assigned to defined dispersions. The most striking feature of the secondary CRs is their almost linear depen-

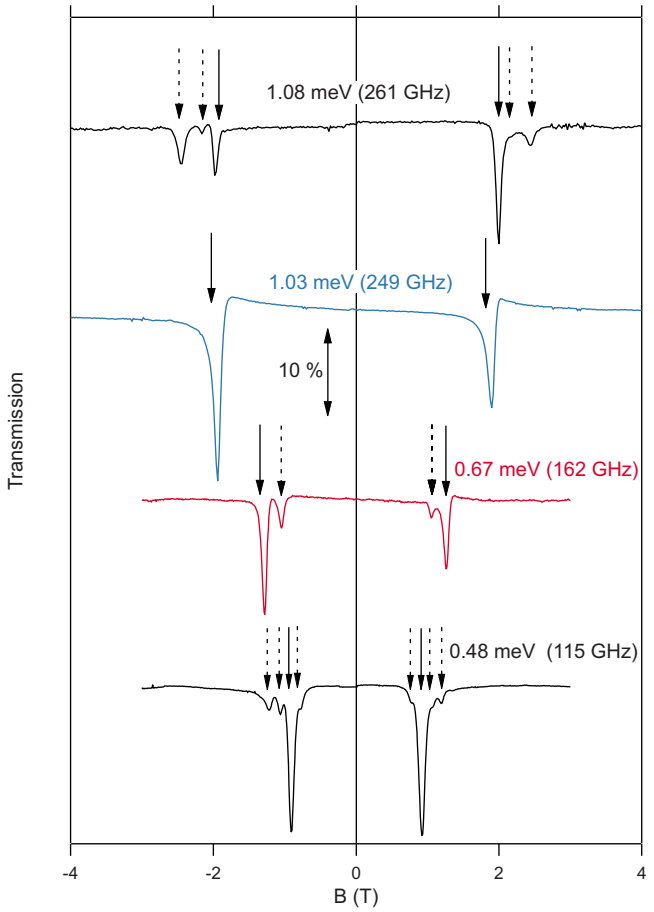

FIG. 3. (Color online) Experimental transmission in the MW regime at $T=1.6$ K for $p_s=1.3\times10^{11}$ cm^{-2}. Multiple CRs are observed. Solid line arrows indicate the main CR, while dashed line arrows indicate secondary CRs. Up to three secondary CRs can be resolved simultaneously and followed over certain B regimes.

dence on the magnetic field B analogous to the magnetic-field dispersion of the main CR. This is in contrast to the behavior of the main CR at $B>4$ T as described above. This results in almost constant cyclotron masses m_c for the secondary CRs, which is, however, different for every p_s. The different m_c are almost equidistant, which is especially well pronounced for $p_s=1.3\times10^{11}$ cm^{-2}. In more detail a slight increase in m_c for decreasing B is found for all hole densities. This has also been observed for the main CR. An exception appears for $p_s=1.6\times10^{11}$ cm^{-2} between 3.3 and 4 T, where a strong decrease in m_c by more than 20% is found. Exceptionally, this secondary CR has an absorption strength ranging between 30% and 70% of the main CR.

For all hole densities one secondary CR was always detected with an energy higher than that of the main CR. Two dispersions at energies lower than that of the main CR are observed for $p_s=1.3\times10^{11}$ and 0.7×10^{11} cm^{-2}. For $B<1.5$ T, however, these two dispersions cannot be resolved separately. A fourth secondary CR rudimentary evolves at still lower energy for $p_s=1.3\times10^{11}$ cm^{-2}. For $p_s=1.6\times10^{11}$ cm^{-2} only one dispersion of the secondary CR can be observed which has lower energy than the main CR. The energy difference between this secondary CR and the main CR is much higher than the corresponding energy differences obtained at the other hole densities. We want to point out that there is no obvious dependence of the position or of the appearance of the secondary CRs on the position of integer filling factors ν observable for $\nu>1$ for all hole densities.

A striking difference between the measurements at different hole densities concerns the values of the corresponding cyclotron mass m_c. As already described before, an increase in m_c with increasing hole density p_s can be observed for the main CR. This behavior is found for the secondary CRs, too: the secondary CRs which have a lower energy than the main CR yield a maximum cyclotron mass of $0.24m_e$ for $p_s=0.7\times10^{11}$ cm^{-2}, $0.30m_e$ for $p_s=1.3\times10^{11}$ cm^{-2}, and $0.41m_e$ for $p_s=1.6\times10^{11}$ cm^{-2}. The deduced cyclotron mass for the secondary CR of higher energy is roughly $m_c=0.17m_e$ for $p_s=0.7\times10^{11}$ cm^{-2}, $m_c=0.19m_e$ for $p_s=1.3\times10^{11}$ cm^{-2}, and $m_c=0.22m_e$ for $p_s=1.6\times10^{11}$ cm^{-2}.

IV. SELF-CONSISTENT BAND-STRUCTURE CALCULATIONS

There are several calculations for the band structure and Landau levels in 2DHS using different models.[1–3,27,28] However, to adopt such calculations directly to our sample parameters and magnetic field and to test the influence of several parameters, which are not exactly known, we have set up a formalism, following the guidelines given in Ref. 28.

We first calculate the subband dispersion for $B=0$ T. For this purpose we use the 4×4 Luttinger Hamiltonian,[21] which includes the topmost fourfold valence band Γ_8 of HH and LH, in the envelope function approximation. The contributions of higher bands are included in the Luttinger parameters γ_1, γ_2, and γ_3. We use the axial approximation, i.e., the "warping" term proportinal to $(\gamma_2-\gamma_3)$ is neglected. Thus, we consider an isotropic case. The z axis is set in the growth directions (001). For this growth direction the hole states are pure with respect to spin for the in-plane wave vector $k_\parallel=0$, i.e., the z component of angular momentum of the HH states is $m=\pm3/2$ and that of the LH states is $m=\pm1/2$. We self-consistently solve the Poisson equation for obtaining the Hartree potential[4] and solve the Schrödinger equation using a quadrature method.[29] The exact shape of the doping region has no significant influence on the band structure. We use as input parameters the depletion charge N_{depl} and the experimentally determined p_s. The not exactly known N_{depl} is set to 1×10^{10} cm^{-2}, but its value does not significantly influence the results. We use the usual parameters for the band offset in the quantum-well system.[30,31] Figure 5 shows the calculated potential profile in the upper part and the subband dispersion in the lower part for $p_s=1.3\times10^{11}$ cm^{-2} and $T=0$ K. Note that the energy grows in the negative direction for holes. The strongly nonparabolic subband dispersion is due to the mixing between HH and LH states for finite $k_\parallel$. The inversion asymmetry of the potential due to the asymmetrical doping yields the spin splitting of the subbands.[1]

The density-of-states effective mass m_{DOS} is displayed in Fig. 6. In the isotropic case it is defined by[4]

$$\frac{m_{\mathrm{DOS}}(E)}{m_e}=\frac{\hbar^2}{m_e}\frac{k_\parallel(E)}{|dE(k_\parallel)/dk_\parallel|}. \tag{2}$$

Two different m_{DOS} are obtained corresponding to the spin-split topmost heavy-hole subband. We think that it is inter-

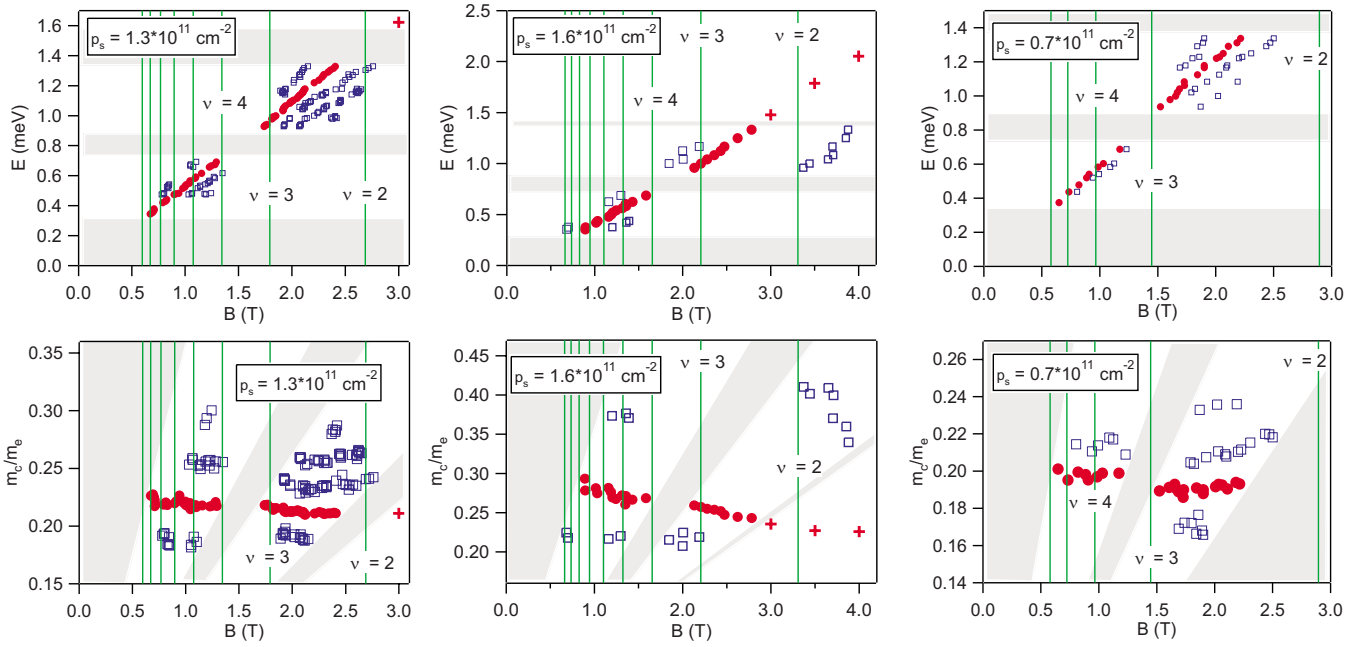

FIG. 4. (Color online) Magnetic-field dependence of the main and secondary cyclotron resonances' energy E and the resulting cyclotron mass m_c for low $B<4$ T measured at $T=1.6$ K for three different hole densities p_s ranging from 0.7×10^{11} to 1.6×10^{11} cm^{-2}. Shaded areas indicate the frequency gaps of the experimental setup. (Red) crosses denote the main CR measured in the FIR regime and (red) closed circles denote those measured in the MW regime. (Blue) open squares indicate the energy of the secondary CRs measured in the MW regime. The positions of integer filling factors ν are indicated by perpendicular lines.

esting to note that m_{DOS} evolves from a value close to the LH mass of bulk $(0.083m_e)$ and develops to that of the HH mass of bulk $(0.592m_e)$ with decreasing E or correspondingly increasing $k_{\|}$ (not shown).

For the calculation of the Landau levels we consider the magnetic field B applied parallel to the growth direction. The components of the in-plane wave vector of the Luttinger Hamiltonian are replaced with Landau raising and lowering operators.[21,32,33] The Zeeman term proportional to the isotropic hole g factor κ is added to the diagonal elements, whereas the Zeeman term proportional to the anisotropic hole g factor q is neglected.[3] We additionally take the Hartree potential obtained from the calculations for $B=0$ T.

Following Ref. 28 we calculate the Landau levels using again a quadrature method.[29] The Landau levels evolving from the spin-split highest heavy-hole subband levels are shown in the upper part of Fig. 7. The Landau levels are labeled by the quantum number[32,33] $N^{\pm}$ with $N=n+m+3/2$ and + or − corresponding to the sign of the dominant z component of angular momentum $(m=\pm3/2)$ for $B\rightarrow0$ T following Ref. 34. The Fermi energy E_F was calculated at $T=0$ K. Due to the band-mixing effects the Landau levels depend strongly nonlinear on B.

V. DISCUSSION

For the comparison between the calculations and the experimental results we consider dipole transitions between the Landau levels. They are possible according to the occupation of the Landau levels and according to the selection rule[32,33] for plus polarized radiation $\Delta N=+1$. Since we used unpolarized light in our experiments, transitions for minus polarization following the selection rule $\Delta N=-1$ are also possible. They are not considered in the first part of our discussion because they lie in a regime of much higher energy (around 6 meV) and have small transition probabilities. The resulting selection rule $\Delta N=\pm1$ is valid in the axial approximation. In principle, transitions between Landau levels with different dominant characters (+ or −) are possible, whereas the transition probabilities between these levels are small. Therefore we neglect these transitions in the first part of the discussion. At first we also neglect the possible additional transitions due to thermal occupation ($k_BT=0.138$ meV at $T=1.6$ K) and due to cubic corrections. In the lower part of Fig. 7 the cyclotron masses m_c calculated from the energies of the allowed Landau level transitions are shown together with m_c found in the measurements. Note that the behavior of the calculated m_c follows qualitatively the behavior of the calculated m_{DOS}, i.e., increasing m_c with increasing B and increasing m_{DOS} with decreasing E.

We will first discuss the results obtained at $p_s=1.3\times10^{11}\mathrm{cm}^{-2}$. Due to the nonparabolicity of the hole band structure the calculated Landau-level energies depend nonlinearly on B. The corresponding m_c shows therefore a strong dependence on B and on the positions of the integer filling factors ν. The calculated m_c form a set of two branches corresponding to the different signs of the corresponding Landau-level transitions. However, the calculated m_c varies strongly down to $B<1$ T for each branch. Note that three simultaneous transitions are possible at a certain B for $\nu>2$.

Obviously, the comparison between the calculation and experimental data can be split into two major regions: first, the region with $B>3$ T, where a reasonable qualitative

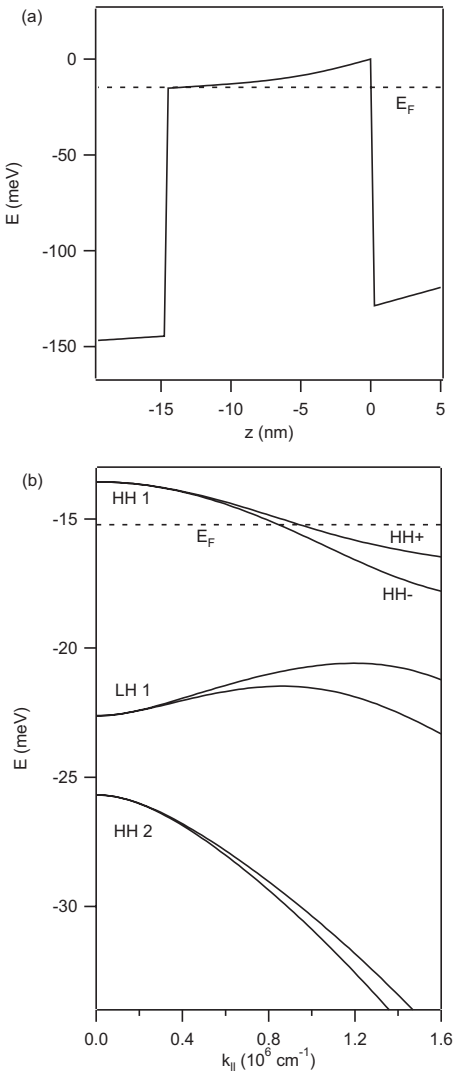

FIG. 5. Calculated (a) potential profile and (b) subband dispersion for $B=0$ T, $p_s=1.3\times10^{11}$ cm^{-2}, and $T=0$ K. The subbands are labeled corresponding to the z component of angular momentum m at $k_{\|}=0$. E_F denotes the Fermi energy.

agreement between theory and experiment can be found, and second, the region with $B<3$ T. Here, the theoretical description fails: the characteristic branches of almost constant and equidistant m_c cannot be reproduced.

A. High magnetic-field regime

We first concentrate on the region with $B>3$ T. Here, the strong decrease in m_c of about a factor of 2 with decreasing B is qualitatively well described by identifying it with the transition $3^+\rightarrow4^+$. We want to point out that the strong B dependence of m_c which we observe, and which is in agreement with theoretical predictions, has not been observed experimentally so far in such a complete and comprehensive manner for two-dimensional hole systems based on GaAs. The continuous set of data in this region was obtained since we use for our experiments a Fourier-transform spectrometer in the FIR regime instead of using FIR lasers with a limited number of laser lines.

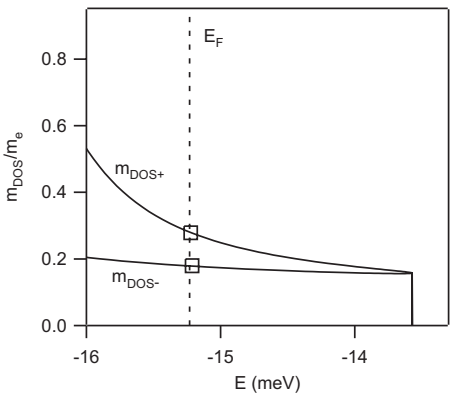

FIG. 6. Calculated density-of-states effective mass m_{DOS} of the topmost subband. $m_{\mathrm{DOS+}}$ and $m_{\mathrm{DOS-}}$ correspond to the upper and lower spin subbands of Fig. 5.

The bending of m_c at $B=3$ T may be attributed to the transition $0^-\rightarrow1^-$. If this is the case two resonances should be resolved. This is not observed in our measurements. However, the observed broadening of the resonance, as described in Sec. III, may be due to a superposition of the transitions $3^+\rightarrow4^+$ and $0^-\rightarrow1^-$ which cannot be resolved separately. We will come back to this point later.

It should be noted that we use a simplified model in our calculation, i.e., we use the axial approximation and neglect the split-off band. In addition, we use the Hartree approximation and do not involve the complete potential structure as described in Sec. IV. Taking these simplifications into account, the remaining quantitative difference of the calculated m_c corresponding to the transition $3^+\rightarrow4^+$ remains justifiable.

In the following we will discuss the influence of the not exactly known parameters which are involved explicitly in the calculations. As it was already mentioned in Sec. IV the results of the calculation of the band structure depend on the set of Luttinger parameters γ_1, γ_2, and γ_3 for GaAs. For the calculation of the Landau levels the effective g factor κ additionally plays an important role. Examples for different sets of Luttinger parameters are given in Table I. They were deduced from measurements[35,36] or calculated on the basis of the more precisely known Luttinger parameters of Ge.[37] In our calculations we used the well-established[1,3,27] set of Hess *et al.*[35] Taking the set of Lawaetz *et al.*[37] changes m_c by less than 0.5%. The effect of varying the sets of Luttinger parameters of Hess *et al.*[35] and of Shanabrook *et al.*[36] is shown in Fig. 8. With the set of Shanabrook *et al.*[36] the quantitative mismatch is reduced compared to the calculations based on the set of Hess *et al.*,[35] whereas the slope of the dispersion is less well reproduced. However, it should be noted that Sha-

TABLE I. Different sets of Luttinger parameters $\gamma_1, \gamma_2, \gamma_3$ which were used in the calculation of m_c in Fig. 8.

Reference	γ_1	γ_2	γ_3
Hess (Ref. 35)	6.85	2.10	2.90
Shanabrook (Ref. 36)	6.8	1.9	2.73
Lawaetz (Ref. 37)	7.65	2.41	3.28

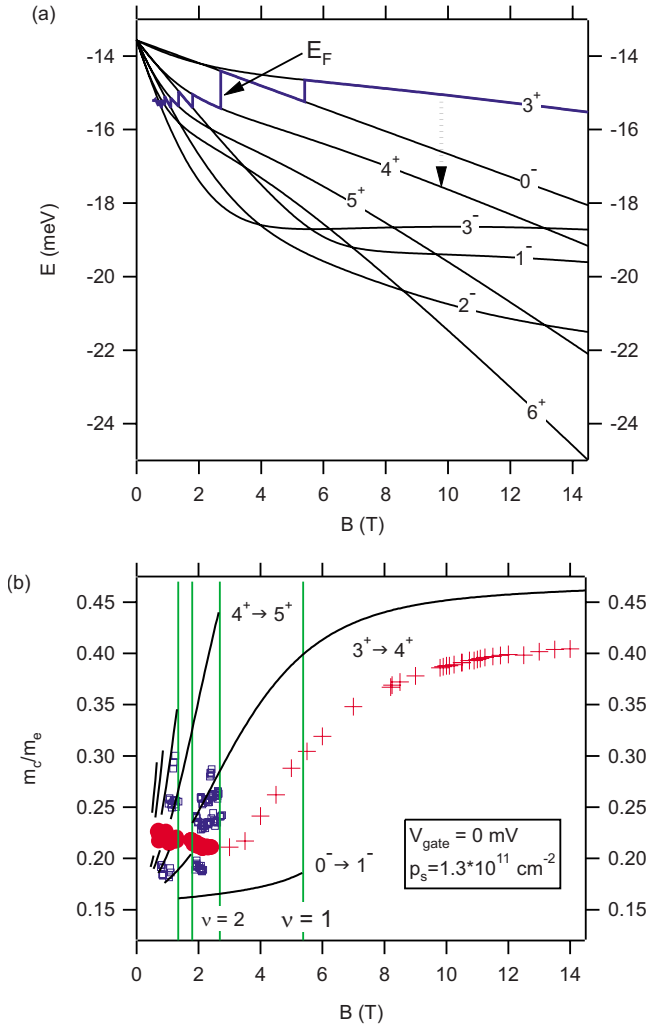

FIG. 7. (Color online) (a) Calculated Landau levels evolving from the spin-split highest heavy-hole subband together with the Fermi energy E_F (bold blue line). One possible transition of the CR is indicated by the dashed arrow. (b) Corresponding calculated cyclotron masses m_c (solid line) and measured m_c (markers) for $p_s = 1.3\times10^{11}$ cm^{-2}. (Red) crosses denote the m_c calculated from the main cyclotron resonance CR measured in the FIR regime and (red) closed circles denote those measured in the MW regime. (Blue) open squares indicate the m_c deduced from the secondary CRs measured in the MW regime. The details of the regime $B<3$ T will be shown later.

nabrook *et al.*[36] did not deduce a value for κ, which we therefore set to $\kappa=1.2$ for this comparison as it was measured by Hess *et al.*[35]

The depletion charge was set to $N_{\mathrm{depl}}=1\times10^{10}$ cm^{-2}. Changing N_{depl} by 1 order of magnitude yields a change of less than 0.5%. In addition, it turns out that the value of the valence-band discontinuity ΔE_v is not critical in our calculations: a change in ΔE_v by 30% yields a change in m_c by only 0.1%.

As described in Sec. III, m_c shows a strong dependence on p_s for small B, where m_c increases with increasing p_s: between $p_s=0.7\times10^{11}$ and 1.6×10^{11} cm^{-2} an increase in m_c by more than 50% can be observed for small B at the main CR. The dependence of m_c on p_s for high B can be deduced

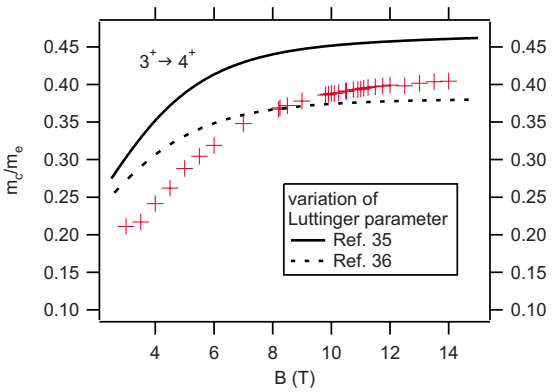

FIG. 8. (Color online) Measured (red crosses) and calculated m_c for different sets of Luttinger parameters.

from Fig. 9. Here, only a small dependence of m_c by a few percents is found with the same tendency compared to the dependence at small B, i.e., increasing m_c with increasing p_s. The calculated m_c, again corresponding to the transition $3^+ \rightarrow 4^+$, shows the same tendency, whereas an overall quantitative difference between calculated and measured m_c is found as in the case for $p_s=1.3\times10^{11}$ cm^{-2} discussed above.

B. Low magnetic-field regime

In the regime of low magnetic fields we only observe a smooth dependence of m_c on B. In this regime, where several Landau levels are occupied, the calculations predict several transitions and therefore several different m_c at a certain magnetic field, as depicted in all parts of Fig. 10. For $\nu>2$ three simultaneous transitions are possible at $T=0$ K. The calculated m_c strongly depend on B and exhibit characteristic cusps and jumps at the positions of the integer filling factors.

However, our measurements show a continuous evolution of the main and secondary branches of m_c in the low-field regime, as it can be seen in Fig. 10. These branches lie much closer to each other than the predicted ones. In addition, the increasing tendency with decreasing B of m_c, which is especially clearly pronounced for $p_s=1.6\times10^{11}$ cm^{-2} [Fig. 10(c)], cannot be explained by the theory. Note that the calculated m_c decrease with decreasing B within between the positions of integer ν.

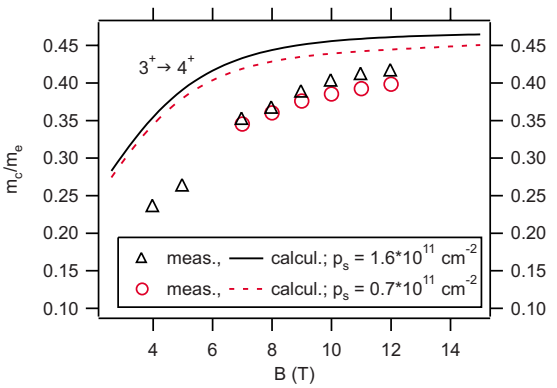

FIG. 9. (Color online) Measured and calculated m_c for two different hole densities p_s. Line styles are given in the inset.

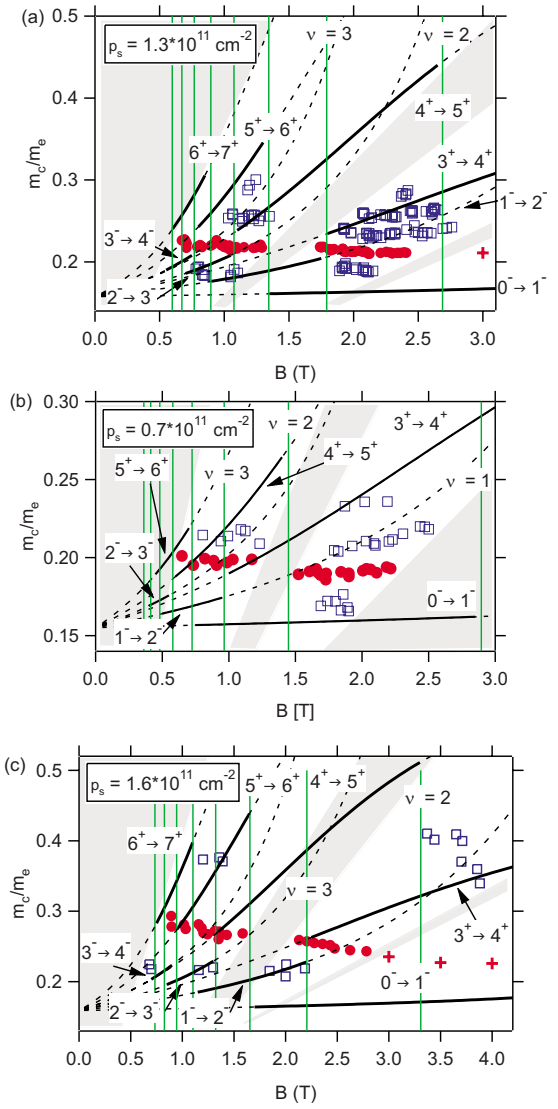

FIG. 10. (Color online) Measured and calculated m_c in the low magnetic-field regime for the hole densities (a) $p_s=1.3\times10^{11}$ cm^{-2}, (b) 0.7×10^{11} cm^{-2}, and (c) 1.6×10^{11} cm^{-2}. (Red) crosses denote m_c extracted from the main cyclotron resonance CR measured in the FIR regime and (red) closed circles denote those measured in the MW regime. (Blue) open squares indicate m_c deduced from the secondary CRs measured in the MW regime. (Black) solid lines indicate the calculated m_c according to the allowed transitions. Dashed lines indicate the calculated m_c, which correspond to forbidden transitions at $T=0$ K due to an empty initial or a completely filled final state. Shaded areas indicate the nonavailable gaps in the MW spectrum of our experimental setup.

We want to point out that the variation of parameters, which was described in Sec. V A, does not lift the discrepancies between the calculations and the measurements. In addition, the absorption strength of the corresponding CR should also strongly depend on B due to different occupations of the Landau levels,[28] whereas this paper dealt with the theoretically comparable material system of SiGe/Ge. The formation of one main CR in our measurements is in contrast to this prediction.

It was shown[27] that additionally including the warping term yields an anticrossing of the Landau levels with $\Delta N = \pm 4$ in the (001) direction. However, such anticrossings should exhibit strong discontinuities[12] and strong changes in the oscillation amplitudes,[28] which we do not observe.

TABLE II. Comparison between the experimental m_c at $B=0.9$ T and the calculated $m_{\mathrm{DOS}\pm}$ for different p_s.

p_s (cm^{-2})	m_c/m_e ($B=0.9$ T)	$m_{\mathrm{DOS}+}/m_e$	$m_{\mathrm{DOS}-}/m_e$
1.3×10^{11}	0.22	0.28	0.18
1.6×10^{11}	0.29	0.35	0.18
0.7×10^{11}	0.19	0.20	0.17

It should be noted that the occurrence of the secondary branches of m_c cannot be explained by thermal occupation, which can be deduced for example from part (a) of Fig. 10 for $B<1.4$ T: the dotted lines, which correspond to the forbidden transitions at $T=0$ K, show a similar strong dependence on B as the allowed solid lines.

As described before, the different branches of m_c depend on p_s, i.e., we measured an increase in m_c with increasing p_s. This tendency could be reproduced by the calculations at high magnetic fields. At small B this dependence has been elaborated.[18–20] There, the obtained values of m_c are larger, which can be attributed to the increased width of the quantum wells compared to our samples. It is instructive to compare the value of the m_c corresponding to the main CR at small B with the values of the density-of-states effective mass m_{DOS} at the Fermi energy, since for $B\rightarrow0$ the values of m_c theoretically converge to the values of m_{DOS}. In our measurements only one main CR was observed, so that such a comparison has only a certain qualitative character and a direct identification with $m_{\mathrm{DOS}+}$ or $m_{\mathrm{DOS}-}$ is not possible. Table II shows nevertheless that the values of $m_{\mathrm{DOS}\pm}$ increase also with increasing p_s.

Up to now we have discussed the results in a single-particle picture, i.e., neglecting hole-hole interactions. In high-mobility two-dimensional electron systems of modulation-doped AlGaAs/GaAs heterostructures one also expects in a single-particle picture several CRs arising from transitions between different spin-split Landau levels, which have different separations due to the small but nevertheless remaining nonparabolicity of the system. Surprisingly, this was not observed in first experiments[23] although the linewidth of the CR was small enough to clearly resolve the expected separation. This puzzle was theoretically solved by Cooper and Chalker[38] and elaborated theoretically and experimentally by many authors (see, e.g., Hu *et al.*[39] and references therein). The explanation is that in a nonparabolic system Coulomb interaction couples the different transition thus that the excitation becomes the character of magnetoplasmon modes. Their positions are shifted with respect to the one-particle separations, accompanied by transfer of oscillator strengths leading, for high densities, to just one dominant mode. In Ref. 13 such magnetoplasmon effects in a two-level mode were used to explain their data on 2DHS.

As we work out in the following, we believe that magnetoplasmon or carrier-carrier interaction effects are also important for our experiments where up to four closely separated CRs with smooth B dispersions are observed, despite of

the expected jumps in the one-particle picture at integer filling factors. As mentioned in Sec. V A, our calculations predict two resonances for $1<\nu<2$. We only observe a broadening for $p_s=1.3\times10^{11}$ cm^{-2}. In the regime of low magnetic fields, we observe more than two CRs which are much less separated than the calculated ones. Both observations together with the formation of one main CR may be indications for carrier-carrier interactions. The data of Ref. 13 are described for such low magnetic field that the nonparabolicity does not play a significant role, i.e., m_c is not altered. Our observation of more than two CRs over a magnetic-field range, where the calculated m_c strongly vary, does therefore not allow an application of the above-described model to our measurements.

Additionally, it turned out that in the case of a two-level system there is a strong influence of the temperature on the splitting of the CRs affected by carrier-carrier interaction.[13,38,39] In the low-field regime our measurements show a clear dependence of the CR position on the temperature T, which is another indication for carrier-carrier interactions. As it is shown in Fig. 11, the CRs shift to higher magnetic fields with increasing T. Note that for $T=7$ and 10 K the broadening of the CRs due to the decrease in the mobility does not allow the observation of multiple resonances separately. However, Fig. 11(b) demonstrates that the shifting of the CRs is not reduced with increasing T as observed and explained by Cole *et al.*[13] in the regime of low magnetic fields for 2DHS. It should be noted that the principal mechanism behind the temperature dependence of the CRs is probably the same, i.e., the temperature dependence of the Coulomb scattering which mediates the coupling between the different transitions. Nevertheless, the resulting shifting should be different in the case of three interacting CRs in comparison to a two-level system. A theory describing three interacting transitions does not exist to our knowledge.

The continuous evolution of a main and several secondary CRs in the regime of low magnetic fields, which has not been observed so far, cannot be explained in the axial approximation. We believe that this behavior is caused by a complicated interplay between effects due to intermixing of Landau levels and carrier-carrier interactions which has not been described so far.

C. Cyclotron resonance between Landau levels originating from the two different spin-split heavy- and light-hole subbands

We observe a weak but clearly resolved very sharp CR in the FIR regime at the magnetic quantum limit, where only the lowest-lying Landau level 3^+ is occupied, i.e., $\nu<1$. Experimental spectra are shown in Fig. 12. The resonance position shifts with B. This resonance has less than 10% of the absorption strength of the main CR and disappears around $B<8$ T. Note that the experimentally observed absorption strength is much stronger than the absorption strength of a CR, which could be expected due to thermal occupation of the next Landau level. We do not have any indications of an anticrossing behavior of the CRs as it was observed in Refs. 9 and 10.

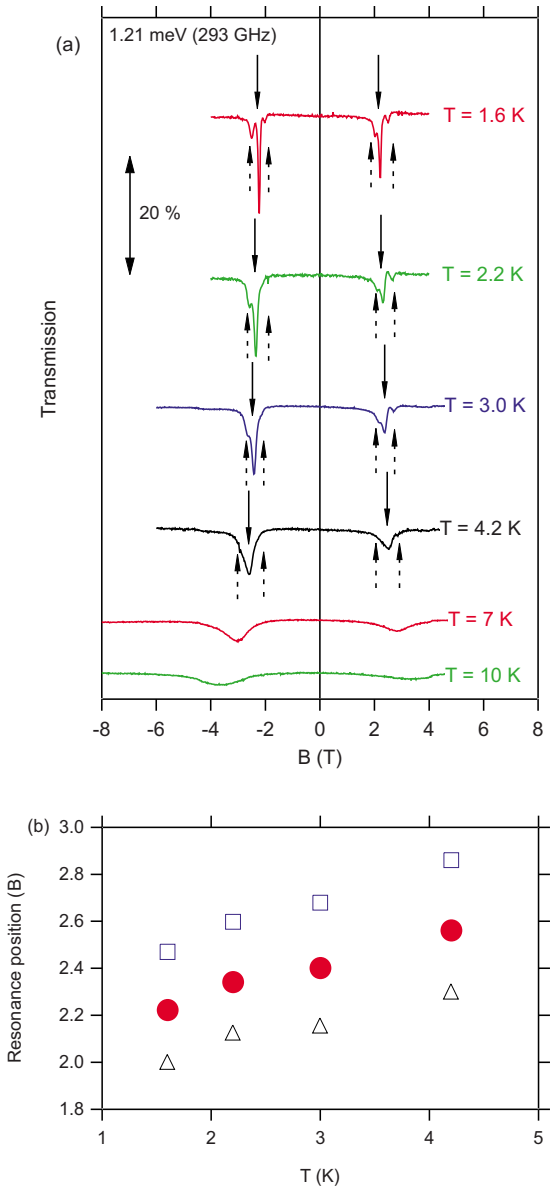

FIG. 11. (Color online) (a) Experimental transmission at 1.21 meV (293 GHz) for different temperatures for $p_s=1.3\times10^{11}$ cm^{-2}. Solid line arrows indicate the main CR, while dashed line arrows indicate secondary CRs. (b) Corresponding resonance positions versus temperature up to $T=4.2$ K. Closed circles indicate the main CR, while open squares (triangles) indicate the higher- (lower-) lying secondary CR.

Up to now we have restricted our discussion to the CRs corresponding to transitions between Landau levels originating from the same subband following the selection rule $\Delta N=+1$ for plus polarization of incident light. Taking also into account minus polarization, transitions with $\Delta N=-1$ are possible. Theoretically, transitions with small absorption strength between Landau levels originating from different subbands, e.g., the spin-split heavy-hole subbands are possible.[3] These transitions are allowed due to the mixing of the Landau levels resulting from the mixing of the subbands. The transition probabilities depend on the portion of the same z component of angular momentum m in the initial and

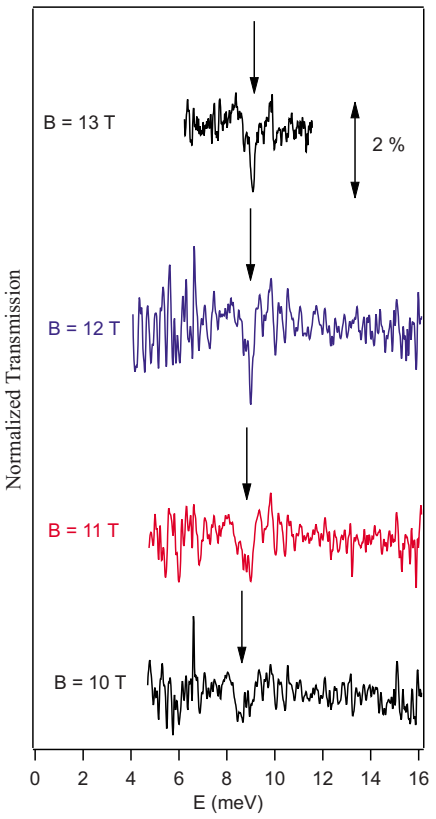

FIG. 12. (Color online) High-energy CR in the FIR regime, measured for $p_s = 1.3 \times 10^{11}$ cm^{-2} at $T = 1.6$ K.

final Landau levels and the overlap of the envelope functions in the z direction. Therefore, the transition probability between a Landau level originating from the lowest-lying HH1 subband and that originating from the first excited HH2 subband is smaller than a transition to a Landau level originating from the lowest-lying LH1 subband, irrespective of the particular portion of m. Direct transitions between Landau levels originating from different subbands have not been clearly observed so far to our knowledge, but transitions were observed which were attributed to anticrossings between Landau levels originating from HH1 and LH1 subbands.[10,11]

In addition, the selection rule $\Delta N = \pm 1$ is only valid in the axial approximation. It turned out that beyond the axial approximation transitions are possible with $\Delta N = \pm i$, where i is an odd integer.[3,32,33] Such transitions of higher order have not been observed yet either.

The corresponding magnetic-field dependence of m_c is shown in Fig. 13 for two different p_s. In addition the possible calculated branches of m_c are on display, according to the indicated transitions. The transitions are labeled as in Sec. IV and LH denotes the transition to a Landau level originating from the LH1 subband. All these corresponding calculated transitions mediate between Landau levels originating from different subbands and are reasonably close to the measured ones. Note that in contrast to the CRs described above all calculated branches have smaller values of m_c for the higher p_s as it was also observed experimentally. Therefore it seems to be evident that we indeed observed a transition between Landau levels originating from the two different spin-split heavy- and light-hole subbands.

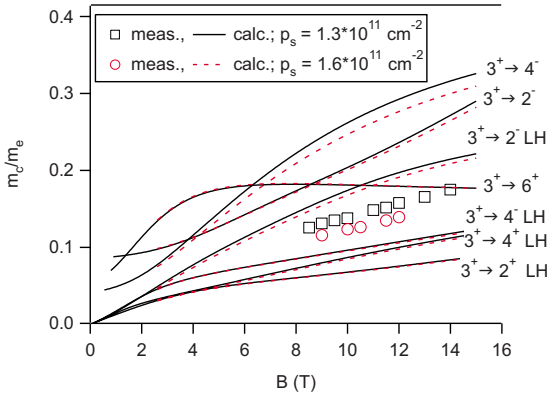

FIG. 13. (Color online) Magnetic-field dependence of the m_c of the measured second CR in the FIR regime and the calculated m_c, which are possible according to the denoted transitions. The results for $p_s = 1.3 \times 10^{11}$ and 1.6×10^{11} cm^{-2} are on display. The linewidth is implicitly indicated by the thickness of the symbols. Line styles are given in the inset.

However, it is not clear, which is the actual transition. According to the portions of the same m in the initial and final states, it turns out that the transitions $3^+ \rightarrow 4^-$ and $3^+ \rightarrow 4^+$LH are most likely. The transition $3^+ \rightarrow 6^+$, which is possible beyond the axial approximation, shows the smallest difference when changing p_s and may therefore not be the underlying transition. However, the other transitions cannot be excluded. The disappearance of the CR with decreasing B is probably due to a continuous decrease in the mixing between the Landau levels.

Since our observed CRs are surprisingly very sharp compared to the range of possible transitions, a simple superposition of all possible resonances cannot hold as an expression. As discussed in Sec. V B carrier-carrier interactions have strong influences on the CRs. Here, it seems that carrier-carrier interactions couple the possible CRs to a single magnetoplasmon mode. In that case there would have been observed a coupled magnetoplasmon mode of CRs, which correspond to transitions between Landau levels originating from both heavy- and light-hole subbands.

D. Temperature dependence of the mobility

It is well known that high-quality two-dimensional electron systems (2DESs) show a significant temperature dependence of the zero-field transport mobility μ_{tr} below $T = 4.2$ K (Ref. 40) due to reduced phonon scattering or other scattering mechanisms.[41] Such behavior has also been observed in 2DHS.[42] Another important aspect concerning μ_{tr} is the metal-insulator transition especially in 2DHS.[43,44]

Our samples also exhibit a strong dependence of μ_{tr} on T below 4.2 K as it is shown in the lower part of Fig. 14. μ_{tr} increases from 4×10^5 to 11×10^5 cm^2/V s corresponding to an increase of a factor of 3 with decreasing T from 4.2 to 1.6 K.

It is well known that the cyclotron mobility μ_{CR} deduced from the width of the CR is not necessarily connected with μ_{tr}. Cavity, thermal occupation, or screening[45] effects can significantly influence μ_{CR}. Ando[46] deduced an increase in

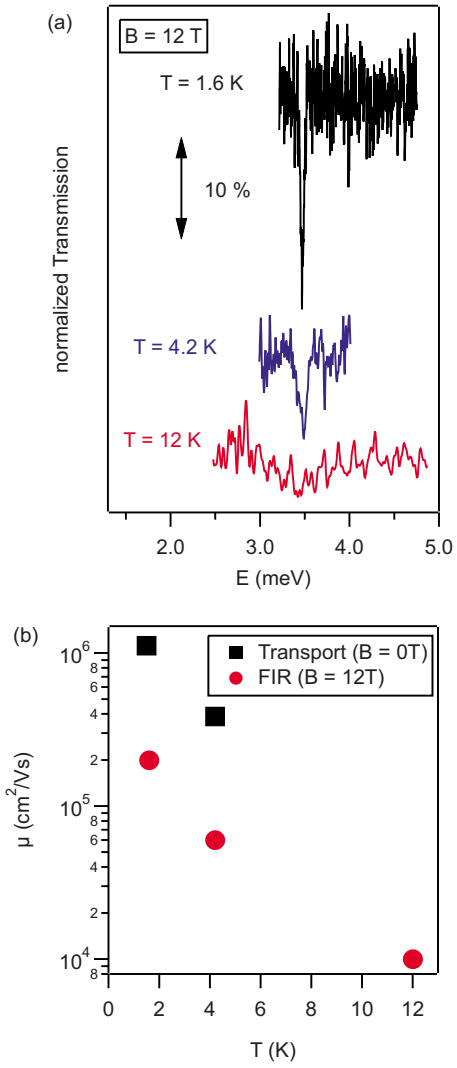

FIG. 14. (Color online) (a) Experimental spectra in the FIR regime at $B=12$ T for different temperatures T. (b) Temperature dependence of the zero-field transport mobility and of the cyclotron mobility. Styles are given in the inset.

the linewidth proportional to $\sqrt{B}$ considering short-range scatterers. It is nevertheless instructive to have a closer look on the cyclotron mobility μ_{CR} in dependence of T. As already mentioned in Sec. V B, the width of the CR in the MW regime increases with T. To deduce a "pure" μ_{CR}, we measured the dependence of μ_{CR} in the magnetic quantum limit at $B=12$ T in the FIR regime for the main CR. It should be noted that in the regime of the magnetic quantum limit μ_{CR} does not depend on B at our samples. The experimental spectra are shown in the upper part of Fig. 14. Interestingly, the resulting cyclotron mobility μ_{CR} shows roughly the same amount of an increase of a factor of 3 when decreasing T from 4.2 to 1.6 K. Note that the values of μ_{CR} have an amount of only 20% of μ_{tr} which cannot completely be attributed to the resolution of our Fourier-transform spectrometer (3.7 μeV). Consequently, quantitative differences between the absolute values of μ_{tr} and μ_{CR} remain whereas the temperature dependence is equal.

Another interesting aspect is that there is no dependence of the position of the CR in the magnetic quantum limit found up to $T=12$ K. This is in contrast to the strong temperature dependence of the position of the main CR on T in the regime of low magnetic fields. Since in the magnetic quantum limit only one main CR can be expected, this may be a further indication of coupling phenomena in the regime of low magnetic fields.

VI. CONCLUSIONS

We have measured the cyclotron resonance in high-quality carbon-doped 2DHS with tunable hole density over a wide frequency regime covering the microwave and FIR regimes. For the comparison with theory we performed self-consistent one-particle calculations of the band structure and the Landau levels based on a 4×4 Luttinger Hamiltonian in the axial approximation.

In the regime of high magnetic field we observe one main CR yielding a strong dependence of m_c on B demonstrating the high nonparabolicity of the 2DHS. This behavior can be reproduced by the calculations in a reasonable agreement considering the involved approximations.

In the regime of low magnetic field we observe a rich spectrum of sharp resonances with well-defined continuous magnetic-field dispersion. One main and up to three additional secondary CRs are observed, which do not show any cusps or jumps at the positions of the integer filling factors. The occurrence of several closely spaced CRs has not been observed before or theoretically predicted.

In a comparison with our calculations we cannot explain this experimental finding. Rather we believe that there has to be considered both the mixing of Landau levels beyond the axial approximation and the coupling of the inter-Landau-level transition, which have the character of magnetoplasmons in the strongly nonparabolic system.

In addition, we observe a sharp additional CR with low absorption strength in the regime of high magnetic field, which disappears with decreasing B. The comparison with the calculation reveal that this CR is due to a transition between Landau levels originating from the two different spin-split heavy- and light-hole subbands. Since from the calculation several transitions are possible in this regime, which are not observed separately, we take this again as a strong indicator for a coupling of the corresponding transitions.

Finally we demonstrated a close relationship between the zero-field transport and the cyclotron mobility in the magnetic quantum limit. Both show an increase of a factor of 3 when decreasing T from 4.2 to 1.6 K.

ACKNOWLEDGMENTS

The authors N. Mecking and P. Moraczewski for helpful discussions. Financial support of the Deutsche Forschungsgemeinschaft via the SFB 508 "Quantum Materials" and the Graduiertenkolleg 1286 "Functional Metal-Semiconductor Hybrid Systems" is gratefully acknowledged.

*kevin.rachor@physnet.uni-hamburg.de

[1] D. A. Broido and L. J. Sham, Phys. Rev. B **31**, 888 (1985).
[2] E. Bangert and G. Landwehr, Superlattices Microstruct. **1**, 363 (1985).
[3] U. Ekenberg and M. Altarelli, Phys. Rev. B **32**, 3712 (1985).
[4] R. Winkler, *Spin-Orbit Coupling Effects in Two-Dimensional Electron and Hole Systems* (Springer, Berlin, 2003).
[5] J. P. Kotthaus and R. Ranvaud, Phys. Rev. B **15**, 5758 (1977).
[6] H. L. Störmer, Z. Schlesinger, A. Chang, D. C. Tsui, A. C. Gossard, and W. Wiegmann, Phys. Rev. Lett. **51**, 126 (1983).
[7] Z. Schlesinger, S. J. Allen, Y. Yafet, A. C. Gossard, and W. Wiegmann, Phys. Rev. B **32**, 5231 (1985).
[8] B. E. Cole, J. M. Chamberlain, M. Henini, T. Cheng, W. Batty, A. Wittlin, J. A. A. J. Perenboom, A. Ardavan, A. Polisski, and J. Singleton, Phys. Rev. B **55**, 2503 (1997).
[9] Z. Schlesinger and W. I. Wang, Phys. Rev. B **33**, 8867 (1986).
[10] K. Hirakawa, Y. Zhao, M. B. Santos, M. Shayegan, and D. C. Tsui, Phys. Rev. B **47**, 4076 (1993).
[11] S. J. Hawksworth, S. Hill, T. J. B. M. Janssen, J. M. Chamberlain, J. Singleton, U. Ekenberg, G. M. Summers, G. A. Davies, R. J. Nicholas, E. C. Valadares, M. Henini, and J. A. A. J. Perenboom, Semicond. Sci. Technol. **8**, 1465 (1993).
[12] S. Hill, B. E. Cole, J. Singleton, J. M. Chamberlain, P. J. Rodgers, T. B. J. M. Janssen, P. A. Pattenden, B. L. Gallagher, G. Hill, and M. Henini, Physica B **211**, 440 (1995).
[13] B. E. Cole, F. M. Peeters, A. Ardavant, S. O. Hill, J. Singleton, P. J. Rodgers, W. Batty, J. M. Chamberlain, A. Polisskii, M. Henini, and T. Cheng, J. Phys.: Condens. Matter **9**, 3163 (1997).
[14] B. E. Cole, W. Batty, J. Singleton, J. M. Chamberlain, L. Li, L. van Bockstal, Y. Imanaka, Y. Shimamoto, N. Miura, F. M. Peeters, M. Henini, and T. Cheng, J. Phys.: Condens. Matter **9**, 4887 (1997).
[15] A. D. Wieck and D. Reuter, Inst. Phys. Conf. Ser. **166**, 51 (2000).
[16] M. J. Manfra, L. N. Pfeiffer, K. W. West, R. de Picciotto, and K. W. Baldwin, Appl. Phys. Lett. **86**, 162106 (2005).
[17] C. Gerl, S. Schmult, H. P. Tranitz, C. Mitzkus, and W. Wegscheider, Appl. Phys. Lett. **86**, 252105 (2005).
[18] M. N. Khannanov, I. V. Kukushkin, S. I. Gubarev, J. Smet, K. von Klitzing, W. Wegscheider, and C. Gerl, JETP Lett. **85**, 242 (2007).
[19] H. Zhu, K. Lai, D. C. Tsui, S. P. Bayrakci, N. P. Ong, M. Manfra, L. Pfeiffer, and K. West, Solid State Commun. **141**, 510 (2007).
[20] T. M. Lu, Z. F. Li, D. C. Tsui, M. J. Manfra, L. N. Pfeiffer, and K. W. West, Appl. Phys. Lett. **92**, 012109 (2008).
[21] L. M. Luttinger, Phys. Rev. **102**, 1030 (1956).
[22] F. Thiele, U. Merkt, J. P. Kotthaus, G. Lommer, F. Malcher, U. Rössler, and G. Weimann, Solid State Commun. **62**, 841 (1987).
[23] K. Ensslin, D. Heitmann, H. Sigg, and K. Ploog, Phys. Rev. B **36**, 8177 (1987).
[24] U. Wurstbauer (private communication 2008).
[25] We have developed and optimized this technique in cooperation with T. Krohn and N. Mecking in experiments on magnetoplasmons in 2D electron systems, which will be published separately.
[26] K. Bollweg, T. Kurth, D. Heitmann, E. Vasiliadou, K. Eberl, and H. Brugger, Phys. Rev. B **52**, 8379 (1995).
[27] S. R. Eric Yang, D. A. Broido, and L. J. Sham, Phys. Rev. B **32**, 6630 (1985).
[28] R. Winkler, M. Merkler, T. Darnhofer, and U. Rössler, Phys. Rev. B **53**, 10858 (1996).
[29] R. Winkler and U. Rössler, Phys. Rev. B **48**, 8918 (1993).
[30] *Semiconductors*, Landolt-Börnstein New Series III Vol. 17a, edited by O. Madelung (Springer, Berlin, Heidelberg, 1982).
[31] J. Menéndez, A. Pinczuk, D. J. Werder, A. C. Gossard, and J. H. English, Phys. Rev. B **33**, 8863 (1986).
[32] K. Suzuki and J. C. Hensel, Phys. Rev. B **9**, 4184 (1974).
[33] H. R. Trebin, U. Rössler, and R. Ranvaud, Phys. Rev. B **20**, 686 (1979).
[34] B. B. Goldberg, D. Heiman, M. J. Graf, D. A. Broido, A. Pinczuk, C. W. Tu, J. H. English, and A. C. Gossard, Phys. Rev. B **38**, 10131 (1988).
[35] K. Hess, D. Bimberg, N. O. Lipari, U. Fishbach, and M. Altarelli, in *Proceedings of the 13th International Conference on the Physics of Semiconductors, Rome, 1976*, edited by F. G. Fumi (North-Holland, Amsterdam, 1976), p. 142.
[36] B. V. Shanabrook, O. J. Glembocki, D. A. Broido, and W. I. Wang, Phys. Rev. B **39**, 3411 (1989).
[37] P. Lawaetz, Phys. Rev. B **4**, 3460 (1971).
[38] N. R. Cooper and J. T. Chalker, Phys. Rev. Lett. **72**, 2057 (1994).
[39] C. M. Hu, E. Batke, K. Köhler, and P. Ganser, Phys. Rev. Lett. **75**, 918 (1995).
[40] C. T. Foxon, J. Cryst. Growth **251**, 1 (2003).
[41] J. J. Harris, J. A. Pals, and R. Woltjer, Rep. Prog. Phys. **52**, 1217 (1989).
[42] B. Gribić, C. Ellenberger, T. Ihn, K. Ensslin, D. Reuter, and A. D. Wieck, Appl. Phys. Lett. **85**, 2277 (2004).
[43] Y. Hanein, U. Meirav, D. Shahar, C. C. Li, D. C Tsui, and Hadas Shtrikman, Phys. Rev. Lett. **80**, 1288 (1998).
[44] S. J. Papadakis, E. P. De Poortere, H. C. Manoharan, M. Shayegan, and R. Winkler, Science **283**, 2056 (1999).
[45] D. Heitmann, M. Ziesmann, and L. L. Chang, Phys. Rev. B **34**, 7463 (1986).
[46] T. Ando, J. Phys. Soc. Jpn. **38**, 989 (1975).